ARTICLE

Journal of Materials Chemistry
www.rsc.org/materials

Ultrasmall, small, and wide angle X-ray scattering analysis of diatom biosilica: interspecific differences in fractal properties

Engel G. Vrieling,*[a]† Theo P. M. Beelen,[b] Qianyao Sun,[b] Sandra Hazelaar,[a] Rutger A. van Santen[b] and Winfried W. C. Gieskes[a]

[a]*Department of Marine Biology, Center for Ecological and Evolutionary Studies, University of Groningen, Biological Center, P.O. Box 14, NL-9750 AA Haren, The Netherlands*
[b]*Schuit Institute of Catalysis, Eindhoven University of Technology, P.O. Box 513, NL-5600 MB Eindhoven, The Netherlands*

Received 13th January 2004, Accepted 29th April 2004
First published as an Advance Article on the web 25th May 2004

Freshly prepared acid-cleaned biosilica of 21 different diatom species was studied using a combination of wide, small, and ultrasmall angle X-ray scattering analysis (WAXS, SAXS, and USAXS) in order to determine whether the structural and fractal properties from the subnanometer level up to dimensions of several microns are species-specific, and if so to quantify them. WAXS data are in line with the amorphous nature of this kind of biosilica: no Bragg reflections were observed at the level below 1 nm. Straight domains in the scattering spectra (in both SAXS and USAXS) revealed the presence of different fractal regions with highly species-specific transition points, as part of the surface structure. All silica specimens had four of these fractal regions, but with a length scale per region characteristic for each specimen except for the region (Region I) covering the WAXS domain ($d < 1.5$ nm). In this first region no fractal behavior was observed for the amorphous biosilica. Region II, with a fractal dimension (D_s) over 3.8, which indicates a smooth surface, covered the lower SAXS domain ($1.5 < d < 10$ nm). Region III ($3.3 < D_s < 3.8$), in the upper SAXS and lower USAXS domain ($10 < d < 396$ nm), represented a rougher surface, whereas Region IV ($D_s < 2.8$), the upper USAXS domain ($d > 396$ nm), revealed the roughest surface. Transition points between straight regions in the scattering spectra did relate to the dimension of meso- and macro-pores that are known to be present in diatom biosilica; the pore sizes determined from the spectra agreed with estimates made from electron micrographs. Interestingly, dominant scattering peaks were observed in USAXS, as if we were dealing with crystals as in highly ordered MCM-type silicas. This crystallinity was only apparent, not real; it is most probably due to the high regularity in pore distributions in diatom biosilica in the size range of 100 to $\sim$500 nm. Our data show that diatom biosilica has quantifiable species-specific fractal surface properties, next to the well known species-specific pore architecture that is well beyond those of other well-ordered artificial silica materials. Consequently, it is likely that each also has its own surface pattern of reactive sites and in view of these large variations each diatom species potentially can be the source for the design of a different silica-based material.

Introduction

Micro- and meso-porous silicas and silica-based materials (zeolites, MCM-type materials) are widely used in industrial and technological applications: as fillers in rubber materials such as in tyres, as catalyst supports, as drying agents, as abrasives, and in separation technologies. For each application a silica with specific properties of mechanical strength, pore volume, pore-size distribution, and specific surface area is required. Currently, the demand for such specific silicas is increasing, resulting in the search for new, improved or alternative silica materials. With respect to the latter category, much attention is nowadays paid to biogenic silica sources because of the great natural diversity in architecture, that is species-specific, and because mild reaction conditions govern silica formation in organisms.[1–3]

The most familiar source of biogenic silica is diatomaceous earth or Kieselguhr, which in fact is a geological deposit of minute exoskeletons that are the remnants of unicellular photosynthesizing microalgae of the group of diatoms. Although diatomaceous earth has been well studied, the application of this type of silica remains limited.[4] The deposits are geologically very old (up to a few hundred million years); processes of aging, sintering, and dissolution have destroyed the detailed structures present in freshly prepared diatom biosilica.[2] Furthermore, diatomaceous earth is often contaminated with other elements such as aluminium,[5,6] making them inappropriate as a catalyst support. Finally, diatomaceous earth contains exoskeletons of a *mix* of different species and thus exhibits heterogeneous physico-chemical properties. At present well over 10,000 diatom species are classified based on the distinct morphological features of the exoskeleton.[7,8] Since so many different diatom species exist and also since their siliceous exoskeletons (the so-called frustules) provide promising features recognized in the architecture,[2,9,10] it is worthwhile to study this biosilica source in more detail. Moreover, diatom silica formation is an attractive model, the analysis of which may well result eventually in biomimicry of natural silicification processes.[1,2,11–14]

Until recently, diatom frustule architecture has been studied nearly exclusively by microscopic methods, with most recently complemented by atomic force microscopy.[15–18] Here we present results of an extensive analysis of freshly prepared

† Present address: Groningen Biomolecular Sciences and Biotechnology Institute, GBB Coordinating Office, University of Groningen, P.O. Box 14, 9750 AA Haren, The Netherlands. E-mail: e.g.vrieling@chem.rug.nl

DOI: 10.1039/b400478g

diatom biosilica using a combination of wide, small, and ultrasmall angle X-ray scattering (WAXS, SAXS, and USAXS, respectively) because we aimed to go into greater detail and to define common features and interspecific differences between diatom species with respect to fractal and structural properties.[19–22] Knowledge at this level is required by material scientists, who seek inspiration from nature for the design and biomimetic synthesis of artificial silicas. The resemblance and differences of biogenic diatom material with artificial silicas (namely MCM-type materials) are highlighted in the present paper.

Experimental

Fresh diatom biosilica was prepared from a variety of centric and pennate diatom species, which were obtained from our own and other (*e.g.* CCMP, West Boothbay Harbor, USA) culture collections as described previously.[23] Uni-algal batch-cultures were established at standard growth conditions[24,25] and cells from dense cultures, the final cell density of which differed per species, were harvested by centrifugation (5 min, 3000 × g), washed three times with milliQ water (conductivity < 18.2 mΩ cm at 25 °C), and stored at −20 °C until further analysis. In addition, diatoms were harvested from monospecific diatom blooms (*Odontella sinensis* and *Biddulphia* spp.) in Dutch coastal waters and from tidal flats of the Dutch Wadden Sea. The harvested cells were treated with concentrated nitric acid for 20 min at 100 °C[26] to remove organic matter (the cell content and the protective casing). After extraction the remaining biosilica was washed thoroughly with milliQ water applying centrifugation (five times each for 5 min at 3000 × g) and the resulting acid-cleaned silica was resuspended in 100% ethanol and dried in air at 60 °C. For the specimen of the centric species *O. sinensis* low-temperature ashing was used to remove organic matter.[27]

All diatom biosilicas were examined for the presence of impurities (*e.g.* salt precipitates) originating as a result of removal of the organic matter. For scanning electron microscopy (SEM), small amounts of dried silica were resuspended in a limited volume (max. 100 μL) of 100% ethanol. A small droplet was layered on a stub and air-dried. Subsequently, the material was sputter-coated with gold (Edwards Scan Coat Six) and examined in a JEOL STM35 scanning microscope. For transmission electron microscopy (TEM), a few μL of silica resuspended in ethanol were mounted on Formvar-coated grids, air-dried, and briefly (5 s) stained with 1.0% (w/v) uranyl acetate. After staining, the grids were again air-dried and examined in a Philips EM201 transmission microscope.

Combined small (SAXS) and wide (WAXS) angle X-ray scattering was performed at Station 8.2 of the Synchrotron Radiation Source at Daresbury Laboratories (Warrington, UK), using a camera length of 0.8 m ($0.4 < Q < 7$ nm^{-1}) and 3.4 m ($0.1 < Q < 2.5$ nm^{-1}) for WAXS and SAXS, respectively. The high intensity of the synchrotron radiation and the position-sensitive detectors allowed simultaneous data collection with a good signal-to-noise ratio every 2 min. A multiwire gas-filled quadrant detector (SAXS) and a curved INEL pressurized gas detector (WAXS) were used. The wavelength for station 8.2 was fixed at 1.54 Å ($\Delta\lambda/\lambda = 4 \times 10^{-3}$). More details of the set-up have been reported by de Moor *et al.*[19,20] For SAXS, the Q-axis of the set-up was calibrated with an oriented specimen of wet rat-tail collagen, while for WAXS a powder of fully crystallized zeolite NaA (Proctor & Gamble) was used. The samples of diatom biosilica were applied as powders and mounted in specially designed rotating sample cells[19–22] between Mylar or Kapton windows. The thickness of the polymer windows was ~10 μm, whereas the sample thickness was less than 0.5 mm. The cells were placed in the X-ray beam and rotated at a speed of 2 rpm.

USAXS experiments were performed at the high-brilliance station ID02 at the European Synchrotron Radiation Facility (ESRF; Grenoble, France) using a Bonse-Hart camera and a configuration with two analyzer crystals to avoid desmearing.[28] The first analyzer crystal (Si(220)) was used to scan the angle with three reflections in the horizontal plane. The second analyzer (Si(111)), with two reflections, was used as collimator in the vertical direction to obtain comparable angular resolution in both horizontal and vertical directions. A NaI scintillator was used as detector, which shows a linear response over four decades of scattering intensity. The covered Q-range at the X-ray wavelength $\lambda = 0.995$ Å, determined from calibration with silver behenate,[29] was $0.001 < Q < 0.3$ nm^{-1}. Scans over successive 2θ ranges were recorded using different degrees of attenuation of the incident X-ray beam, so that the intensities on the detector were in the linear range. A complete spectrum was recorded within 5 minutes. USAXS datasets were corrected for the influence of the rocking curve produced by the set-up.

WAXS, SAXS and USAXS spectra were normalized for the intensity of the X-ray beam and corrected for detector sensitivity prior to background subtraction. The scattering of empty cells with two windows (either of Mylar, Kapton, or mica) was used as background scattering. The final scattering intensities of WAXS, SAXS, and USAXS were plotted as log intensity (I) *vs.* log scattering vector (Q), with I in arbitrary units and Q in nm^{-1} (with $Q = (4\pi/\lambda)\sin(\theta/2)$ where θ represents the scattering angle); the latter equals $d = 2\pi Q^{-1}$ (in nm). For a collection of colloidal spherical particles, the intensities in the SAXS spectra can be approximated by

$$I(Q) = NP(Q)S(Q) \quad (1)$$

where N is the number of particles, $P(Q)$ is the form factor and $S(Q)$ the structure factor.[30,31]

Results

In none of the silicas obtained from the freshly harvested diatoms (either cultured or directly obtained from the sea) clear Bragg reflections appeared, in contrast to the calibration specimen of zeolite NaA. A few examples of all spectra obtained are shown in Fig. 1. Electron microscopy revealed well ordered, occasionally hexagonal, distributions of pores, the size range of the smallest ones in the SAXS region, not in that of WAXS. The total absence of Bragg reflections in the solid siliceous exoskeletons of diatoms was as expected:

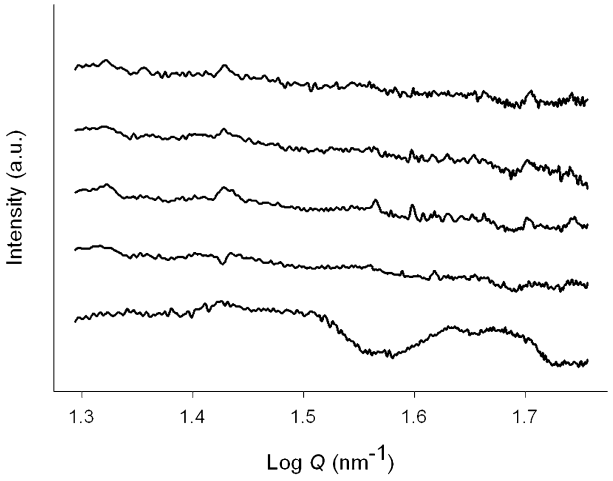

Fig. 1 Examples of WAXS patterns of diatom biosilicas; the spectra are vertically shifted for clarity. From top to bottom the following species are shown: three pennate species *Stauroneis constricta*, *Nitzschia sigma* and *N. closterium* and two centric species *Thalassiosira punctigera* and *T. weissflogii*.

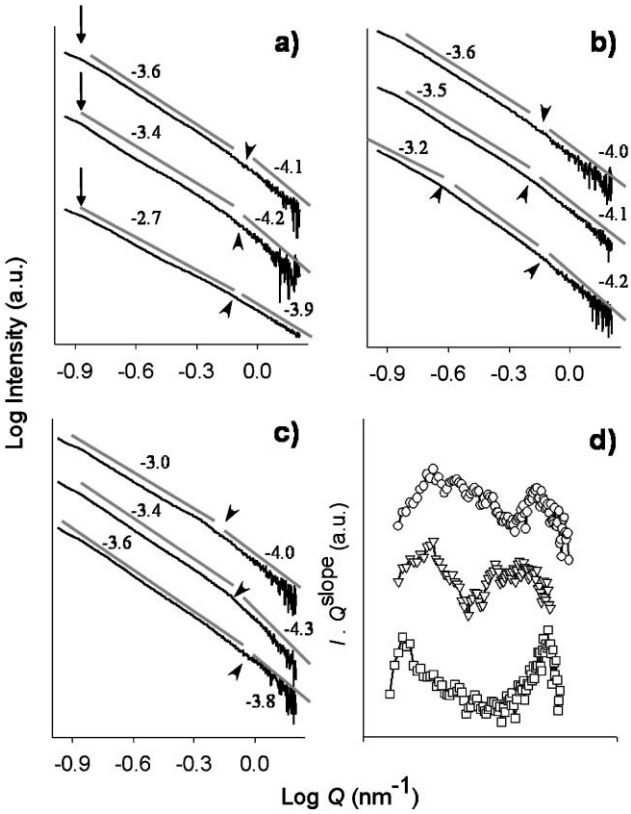

Fig. 2 SAXS patterns of a series of diatom biosilicas: the spectra are vertically shifted for clarity. From top to bottom the following specimens are shown: (a) the centric species *Lauderia borealis, Thalassiosira punctigera*, and *T. weissflogii*.; (b) the pennate species *Nitzschia closterium*, *Skeletonema costatum*, and *Stauroneis constricta*; (c) silica collected from the natural marine environments of the tidal flat of the Wadden Sea (taken in 1995 and 1996, respectively) and from a mono-specific bloom of the centric species *Odontella sinensis* in the North Sea. Note the difference in steepness of the slopes and *q*-domains of the straight regions (marked with grey lines), with the transition points indicated (arrowheads). By canceling out the descending nature of the spectra (d), details on oscillation patterns become more clearly visible as indicated for (○) *L. borealis*, (∇) *S. costatum* and (□) the field sample from 1995. Following this exercise no clear-cut information of hidden dominant peaks was revealed in the SAXS regions.

this type of biosilica is amorphous,[23] as has been suggested earlier.[7,8]

At the upper left of the SAXS spectra the apparent slope transition occurred very close to the upper limit of the SAXS set-up [arrows Fig. 2(a)]. This cannot be ascribed to fractal behavior of the samples. At these low scattering angles the stray scattering of X-rays that hit the beamstop interfere with the measurements; they cannot be cancelled out by background subtraction. Every silica specimen had its own scattering spectrum, indicating that the observed characteristics depend on the individual diatom species. Examples of scattering patterns are shown in Fig. 2; the spectra are of the centric species *Lauderia borealis*, *Thalassiosira punctigera*, and *T. weissflogii* [Fig. 2(a)], the pennate species *Nitzschia closterium*, *Skeletonema costatum*, and *Stauroneis constricta* [Fig. 2(b)], and silica specimens from the natural diatom species collected from tidal flats and from a monospecific bloom in the North Sea [Fig. 2(c)]. Characteristic slope transitions (arrowheads) can be seen, while on some occasions regions with very weak oscillation patterns are present. When the influence of the slope in the descending scattering spectrum is cancelled out by plotting log Q against IQ^{slope}, these oscillations could be examined more precisely. Examples of such weak oscillations are presented from top to bottom for *L. borealis*, *S. costatum*, and a field sample [Fig. 2(d)]. Apparently, no clear-cut dominant peaks were hidden in the overall spectra. Because scattering of our biosilica originates from pores, each transition point indicates the radius of gyration (R_g) of the pores of which the size could be determined with $d = 2\pi Q^{-1}$ (in nm).[13,23] The same pore sizes that were determined by SAXS were recorded in the exoskeletons by electron microscopical observations. Within one species various pore structures and size dimensions can be present, as shown for the species *L. borealis*, *O. sinensis*, *T. weissflogii*, *Navicula salinarum*, and *S. constricta* (Fig. 3).

In comparison to SAXS, the USAXS set-up allowed the extension of the pore size-range study from ~60 nm by SAXS all the way up to ~6,200 nm by USAXS. Due to the overlapping regions—at the lower limit of USAXS and the higher one of SAXS—the spectra from the different set-ups could be merged.[19–22] However, for a better analysis of the scattering in the USAXS domain, we restricted ourselves here to present non-merged data. In agreement with the results obtained with SAXS, each diatom species appeared to have its own scattering pattern in the USAXS domain. Also here the spectra revealed

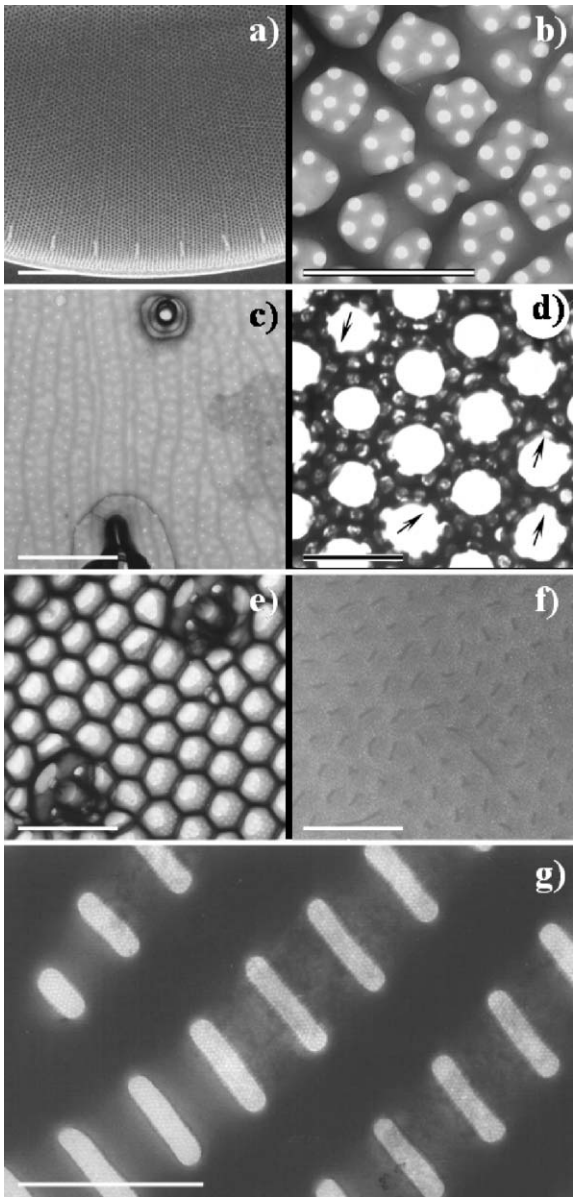

Fig. 3 Electron micrographs of pore structures that are present in the diatom species *Lauderia borealis* (a), *Odontella sinensis* (b), *Thalassiosira weissflogii* (c), *Coscinodiscus granii* (d), *Navicula salinarum* (e), *Nitzschia sigma* (f) and *Stauroneis constricta* (g). Bar measures 5.0 (a) and 0.1 (b–g) micron, respectively.

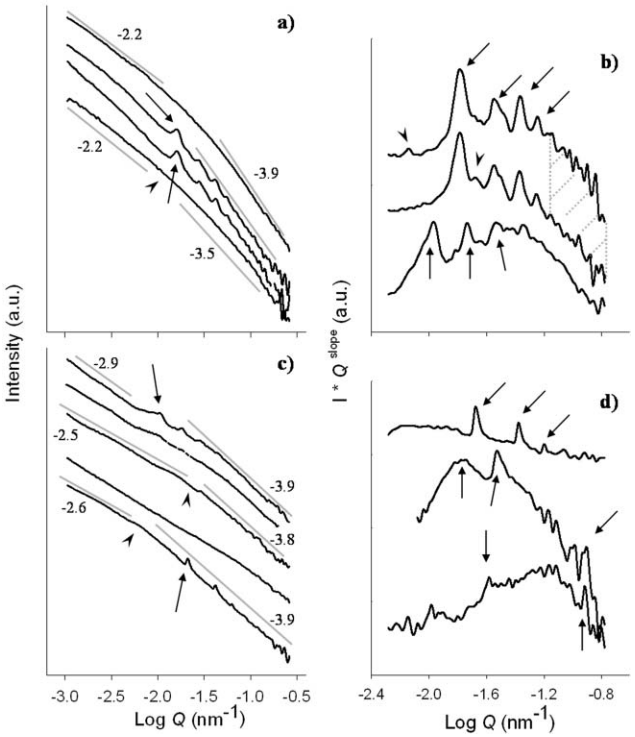

Fig. 4 USAXS patterns of a series of diatom biosilicas; the spectra are vertically shifted for clarity. From top to bottom the following species or samples are shown: (a) the centric species *Ditylum brightwellii*, *Thalassiosira* spp., *T. punctigera*, and *T. weissflogii*; (c) the centric species *Biddulphia* spp. and *Odontella sinensis* collected from different marine blooms, and the pennate species *Navicula cryptocephala*, *N. salinarum*, and *Nitzschia sigma*. Note the differences per specimen in the steepness of slopes (for a few grey lines are shown) and the location of the transition points along the Q-axis (examples are shown by arrowheads). In some occasions, dominant scattering peaks are superimposed on the spectra so they become clearly visible (arrows). By canceling out the descending nature of the spectra (d), details on oscillation patterns become more clearly visible as indicated for (b) the centric species *Thalassiosira punctigera*, *Thalassiosira* spp., and *Biddulphia* spp. and (d) the pennate species *Navicula cryptocephala*, *N. salinarum*, and *Nitzschia sigma*. Note the differences between species in location of dominant scattering peaks (arrows). Between the two *Thalassiosira* species [upper two spectra in (c)], remarkable similarity occurs in the location of the dominant scattering peaks, but differences appear in less dominant peaks (arrowheads and marked region at high log Q values).

multiple straight regions; a few are marked with grey lines in Figs. 4(a) and (c). On some occasions distinct dominant scattering peaks are clearly superimposed on the spectra [arrows in Figs. 4(a) and (c)]. For the centric species *Thalassiosira* spp., *T. punctigera*, *Biddulphia* [Fig. 4(b)] and the pennate species *Navicula cryptocephala*, *N. salinarum*, and *Nitzschia sigma* [Fig. 4(d)], the scattering peaks appeared more clearly when the influence of the slope in the scattering plots was cancelled out in plots of log Q against IQ^{slope}. With this exercise the difference between the silica specimens becomes more obvious. Silica from very closely related diatom species {*e.g.* within the genus *Thalassiosira* [the upper two lines in Fig. 4(b)]} apparently share identical dominant scattering peaks. However, less dominant features still do distinguish such species [arrowheads and the marked area in Fig. 4(b)].

For the strongest peaks [arrows in Figs. 4(b) and (d)] the Q values can be used to calculate the R_g of scatterers. These were compared with estimates of pores made from electron micrographs. For none of the peaks specific pores could be identified in the range of the determined R_g. Following this observation, the distribution patterns of pores was examined in more detail. For the silicas for which we obtained peaks in the USAXS, it appeared that pore distributions were very uniform, even with hexagonal patterning recognizable in some species, possibly due to crystalline behavior as a result of this regular arrangement. This regular pore distribution forms lattices similar as in true crystal and produce diffraction peaks in USAXS. Similar observations were made for the hexagonally patterned mesopores in MCM-41 type silicas examined by XRD and SAXS.[32,33] The narrowness of the peak depends on the uniformity of the distribution of the pores. The pore distribution patterns as determined here by USAXS are visible in the micrographs presented in Fig. 3; a detailed view of the hierarchical pore distribution in the biosilica of *T. weissflogii* is shown in Fig. 5.

Despite the distinct scattering patterns of each species, the underlying and prominent straight slopes of the form factor [$P(Q)$] of which are very strong, a general pattern can be recognized in all the silica specimens that were studied (Fig. 6). Earlier SAXS analysis allowed the definition of a nanoscale uniformity for diatom biosilicas,[23] and the identification of only two common Q-domains. These domains (Regions I and II) covered the Q-range of $\log Q > -0.2\ \text{nm}^{-1}$ [$d < 10$ nm; Region I with fractal dimension (D_s) > 3.8] and $-0.8 < \log Q < -0.2\ \text{nm}^{-1}$ ($40 > d > 10$ nm; Region II with fractal dimension $3.3 < D_s < 3.8$). Thanks to the addition of WAXS and USAXS data presented here, we can now discriminate the fractal regions more precisely, *i.e.* in four fractal regions (Regions I–IV). The characteristics of these regions are as follows: Region I at $\log Q > 1\ \text{nm}^{-1}$ ($d < 0.63$ nm) is the WAXS domain that has no fractal or structural property, in line with the amorphous nature of the biosilicas examined here. Region II (previously denoted as Region I) is the lower SAXS region at $-0.8 < \log Q < -0.2\ \text{nm}^{-1}$ ($40 > d > 10$ nm) with

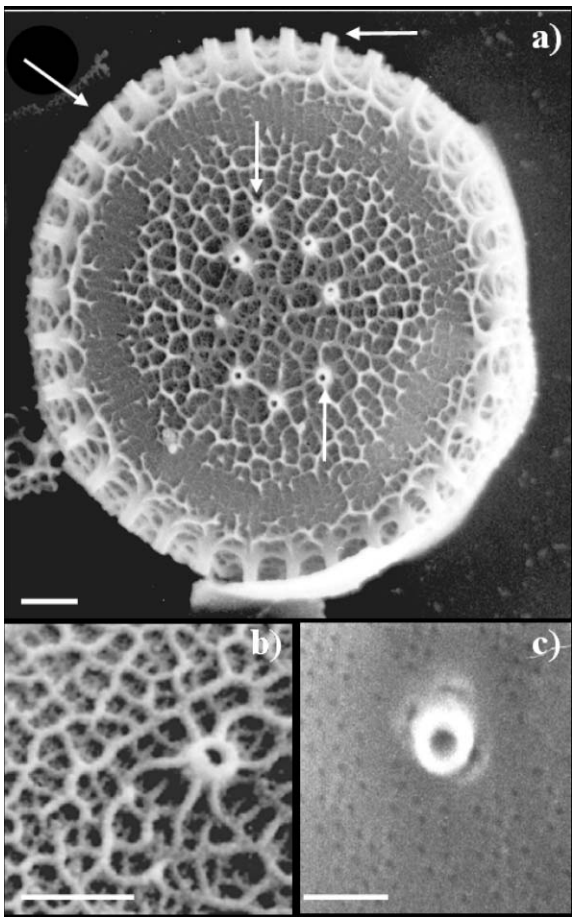

Fig. 5 Hierarchical view of pore dimensions observed within the silica of a single diatom species. Here silica from the centric species *Thalassiosira weissflogii* is shown at three different magnifications. Bar measures 0.1 micron.

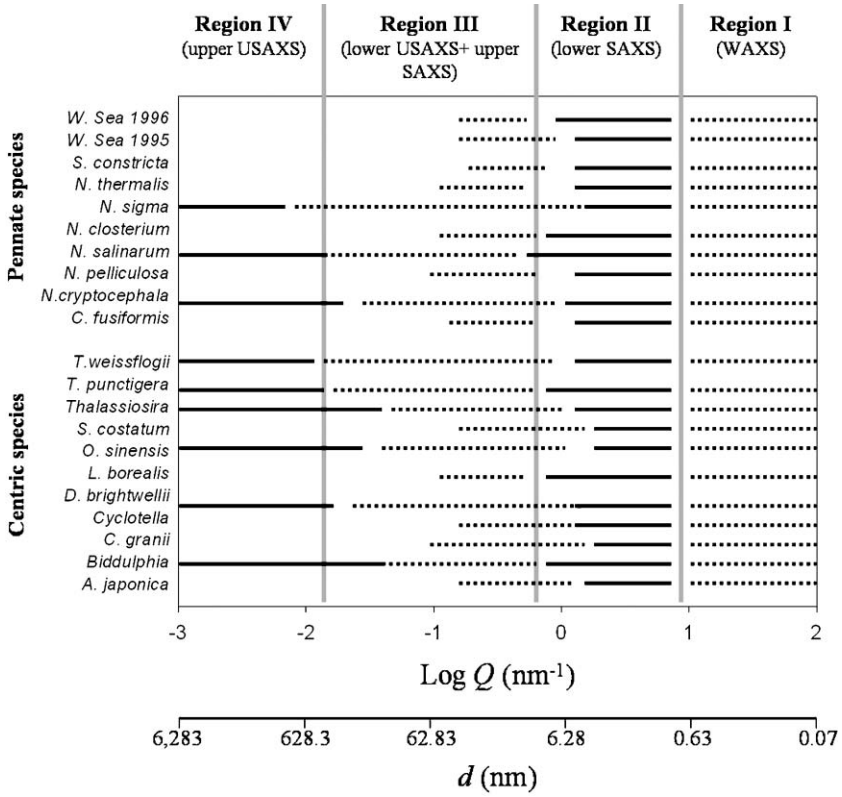

Fig. 6 Nano- and (sub)micronscale uniformity in diatom biosilica determined from the SAXS and USAXS patterns of 21 silica specimens. Four independent Q-domains (Regions I–IV) were assigned to regions where the scattering spectra revealed quite similar slopes. Region I indicates the WAXS region at $\log Q > 1\ \mathrm{nm}^{-1}$ ($d < 0.63$ nm); in this region fractal and structural properties are absent. Region II is the Porod region in the lower SAXS range with a Q-domain of $1 > \log Q > -0.2\ \mathrm{nm}^{-1}$ ($0.63 < d < 10$ nm) with slopes of -3.8 to -4.0. Region III overlaps the upper SAXS and lower USAXS domains from $-1.8 < \log Q < -0.2\ \mathrm{nm}^{-1}$ ($396 > d > 10$ nm) with slopes between -3.3 to -3.8. Region IV indicates upper USAXS range with a Q-domain from $\log Q < -1.8\ \mathrm{nm}^{-1}$ ($d > 396$ nm) and slopes between -2.2 to -2.8. Regions I–III are at the (sub)nanoscale level and Region IV at the submicron level.

$D_s = 3.8$. Region III (previously Region II) stretches from the upper SAXS into the lower USAXS domains, indicating that earlier determined scattering properties by SAXS must be extended substantially into the USAXS domain. This extension confirms that structure (S) and form (P) factors [eqn. (1)] span a much larger region than previously determined. In merged SAXS and USAXS spectra (not shown) the steepness of the slopes continued quite fluently in the overlapping Q-domains. This means that the domain of Region III must be much broader as it apparently covers at least the range between $-1.8 < \log Q < -0.2\ \mathrm{nm}^{-1}$ ($396 > d > 10$ nm). Region III has a fractality of $3.3 < D_s < 3.8$, indicative of a much rougher surface in this domain compared to the smooth surface that scatters in Region II ($D_s > 3.8$). In the upper USAXS spectra a new Q-domain (Region IV) was identified at $\log Q < -1.8\ \mathrm{nm}^{-1}$ ($d > 396$ nm) with $D_s < 2.8$. The surface structure appears to be roughest in the upper USAXS domain. Altogether these findings indicate that diatom biosilica also maintains common fractal properties at a submicron and micron level (Fig. 6), not only at the lowest nanometer range.

Discussion

That solid silica exoskeletons of diatom cells are amorphous has been demonstrated in the past;[8,11] it has been confirmed recently by wide angle X-ray scattering analysis[23] and the results presented here are further proof. Crystal lattices that should have resulted in Bragg reflections were not found in any one of the biosilica specimens that were investigated. At the surface, however, substantial quantities of both Q_2 [Si–$(OH)_2$] and Q_3 (Si=OH) states should be present in view of the chemical shifts of the silicon–oxygen bonds seen in ^{29}Si CP NMR.[14,34] The amorphous nature of the biosilica, a feature apparently common to all diatom species studied, should not be confused with the fact already established before: the morphology of the exoskeletons is species-specific and an important key to the taxonomic classification of diatoms.[7,8] The architectural hierarchy covers, as we show here, no less than three decades in size, from the nanometer up to the submicron level (Figs. 5 and 6), with pores that not only differ in shape between species, but also in dimension and size within each single one. The notion that diatom biosilica can be viewed as a solid silica framework with pores is supported by the fact that diatom biosilica has a much lower specific surface area ($<100\ \mathrm{m}^2\ \mathrm{g}^{-1}$) than synthetically prepared micro- and mesoporous silicas.[2,14] Low specific surface areas imply that micropores of less than 1 nm do not occur, or contribute very little to the surface area. In fact, micropores have not been identified by recent atomic force microscopical studies.[15–18]

SAXS and USAXS analysis also revealed the fractal behavior of diatom biosilica, indeed of all species that were studied. This biosilica has four fractal domains, the fractal dimension of which decreases at larger length scales (larger d-values). Diatom biosilica is apparently a multiple fractal system, with a surface of increasing roughness at larger length scales. Although every silica specimen had its own characteristic borders for each fractal domain, they shared overlapping parts assigned as Regions I–IV (Fig. 6). The existence of common regions implies that diatom biosilica has uniform characteristics with respect to fractality whatever the species, a feature that has not been recognized earlier because microscopy is not sufficient when dealing with nanometer-sized structures. With our combined SAXS/USAXS analysis not only the fractal properties of diatom biosilica, but also the size of pores over a long Q-domain has been determined: SAXS analysis indicated that mesopores (in size between 2 and 50 nm) were present in all

species, in view of transitions of straight regions in the SAXS domain, and with USAXS similar transitions also appeared, but at larger length scales, indicating the presence of macropores (in size $>$ 50 nm).

The fact that in USAXS prominent peaks were superimposed on the spectra of some biosilica specimens suggests crystalline behavior. This, however, would be impossible with the amorphous silica backbone as we have seen. Based on the estimated radius of gyration of the peaks just mentioned specific pores cannot be the scattering source. Instead, preferential pore *distributions* may have led to crystal-like scattering patterns. X-Ray diffraction and SAXS studies in MCM-41 and benzene–silica hybrid materials indicated similar hexagonally ordered channels as the source of such X-ray scattering peaks.[32,33,35] In other words, the combination of amorphous silica and uniform distributions of pores is shared by diatom biosilica and highly-ordered mesoporous silicas. The artificial ones are available in a variety of industrial applications, but the promise of biosilica is far greater in view of: i) the species-specificity of fractal characteristics over a huge size range and consequently a large variety in reactive sites at the surface, and ii) the presence of hierachically ordered meso- and macro-pores with dimensions that are well beyond those of artificial silicas. As we show here, each diatom species has potential to be the source for the design of a different silica based material. Indeed, diatom biosilica proved to be attractive as a support material for zeolitization[3] and for the conversion of biogenic silica towards new metal composites through shape-preserving displacement.[36]

Acknowledgements

We thank Dr P.-P. E. A. de Moor (Eindhoven University) and Dr B. U. Komanschek (CCLRC Daresbury, UK) for assistance during SAXS and WAXS. Dr T. Narayanan (ESRF, Grenoble, France) and C. Houssin (Eindhoven University) assisted in USAXS measurements. Beamtime at SRS Daresbury Laboratories (UK) was provided by the CCLRC agreement for synchrotron use. The European Committee granted beamtime for USAXS (proposal No: SC595 and SC790). A. J. van Bennekom of the Royal Netherlands Institute for Sea Research (KNIOZ) provided the low temperature ashed silica specimen of the species *Odontella sinensis*. J. Zagers assisted in electron microscopic analyses. We are grateful to the referees for providing valuable comments. This research was supported (EGV, QS, and SH) by the Technology Foundation STW (grants GBi55.3883 and GFc4983), applied science division of NWO and the technology program of the Ministry of Economic Affairs.

References

1 D. E. Morse, *TIBTECH*, 1999, **17**, 230.
2 E. G. Vrieling, T. P. M. Beelen, R. A. van Santen and W. W. C. Gieskes, *J. Biotechnol.*, 1999, **70**, 39.
3 M. W. Anderson, S. M. Holmes, N. Hanif and C. S. Cundy, *Angew. Chem., Int. Ed.*, 2000, **39**, 2707.
4 R. K. Iler, *The chemistry of silica*, 2nd edn., Wiley, New York, USA, 1979.
5 P. van Capellen and L. Qiu, *Deep Sea Res.*, 1997, **44**, 1109.
6 P. van Capellen and L. Qiu, *Deep Sea Res.*, 1997, **44**, 1129.
7 F. E. Round, R. M. Crawford and D. G. Mann, *Diatoms, the biology and morphology of the genera*, Cambridge University Press, Cambridge, UK, 1990.
8 J. D. Pickett-Heaps, A. M. Schmid and L. A. Edgar, *Progr. Phycol. Res.*, 1990, **7**, 1.
9 G. A. Ozin, H. Yang, I. Sokolov and N. Coombs, *Adv. Mater.*, 1996, **9**, 662.
10 S. Mann and G. A. Ozin, *Nature (London)*, 1996, **382**, 313.
11 R. Gordon and R. W. Drum, *Int. Rev. Cytol.*, 1994, **150**, 243.
12 C. M. Zaremba and G. D. Stucky, *Curr. Opin. Solid State Mater. Sci.*, 1996, **1**, 425.
13 E. G. Vrieling, T. P. M. Beelen, R. A. van Santen and W. W. C. Gieskes, *W. W. C., Angew. Chem., Int. Ed.*, 2002, **41**, 1543.
14 E. G. Vrieling, S. Hazelaar, W. W. C. Gieskes, Q. Sun, T. P. M. Beelen and R. A. van Santen, *Progr. Mol. Subcell. Biol.*, 2003, **33**, 301.
15 S. A. Crawford, M. J. Higgins, P. Mulvaney and R. Wetherbee, *J. Phycol.*, 2001, **37**, 543.
16 N. Almqvist, N. H. Thomson, B. L. Smith, G. D. Stucky, D. E. Morse and P. K. Hansma, *J. Microsc.*, 2001, **202**, 518.
17 F. Noll, M. Sumper and N. Hampp, *Nano Lett.*, 2002, **2**, 91.
18 Q. Sun and E. G. Vrieling, unpublished work.
19 P.-P. E. A. de Moor, T. P. M. Beelen and R. A. van Santen, *Microporous Mater.*, 1997, **9**, 117.
20 P.-P. E. A. de Moor, T. P. M. Beelen, B. U. Komanschek and R. A. van Santen, *Microporous Mesoporous Mater.*, 1998, **21**, 263.
21 P.-P. E. A. de Moor, T. P. M. Beelen and R. A. van Santen, *J. Phys. Chem. B*, 1999, **103**, 1639.
22 Q. Sun, T. P. M. Beelen, R. A. van Santen, S. Hazelaar, E. G. Vrieling and W. W. C. Gieskes, *J. Phys. Chem. B.*, 2002, **106**, 11539.
23 E. G. Vrieling, T. P. M. Beelen, R. A. van Santen and W. W. C. Gieskes, *J. Phycol.*, 2000, **35**, 1044.
24 E. G. Vrieling, T. P. M. Beelen and W. W. C. Gieskes, *J. Phycol.*, 1999, **35**, 548.
25 W. H. van de Poll, E. G. Vrieling and W. W. C. Gieskes, *J. Phycol.*, 1999, **35**, 1044.
26 J. A. Boyle, J. D. Pickett-Heaps and D. B. Czarnecki, *J. Phycol.*, 1984, **20**, 563.
27 A. J. van Bennekom, J. H. F. Jansen, S. J. van der Gaast, J. M. van Iperen and J. Pieters, *Deep Sea Res.*, 1989, **36**, 173.
28 O. Diat, P. Bösecke, J. Lambard and P.-P. E. A. de Moor, *J. Appl. Crystallogr.*, 1997, **30**, 862.
29 D. W. Hua, J. V. D'Souza, P. W. Schmidt and D. M. Smith, in *Characterization of porous solids III. Stud. Surf. Sci. Catal.*, Elsevier Science, Amsterdam, NL, 1994, **vol. 87**, p. 255.
30 J. E. Martin and A. J. Hurd, *J. Appl. Crystallogr.*, 1987, **20**, 61.
31 J. Texeira, in *On growth and form: fractal and non-fractal patterns in physics*, Martinus Nijhoff Publishers, Dordrecht, NL, 1986, p. 145.
32 S. Biz and M. Ocelli, *Catal. Rev. Sci. Eng.*, 1998, **40**, 329.
33 M. V. Landau, S. P. Varkey, M. Herskowitz, O. Regev, S. Pevzner, T. Sen and Z. Luz, *Microporous Mesoporous Mater.*, 1999, **33**, 149.
34 C. C. Perry, in *Biomineralization: chemical and biochemical perspectives*, VCH Publishers, New York, 1989, p. 223.
35 S. Inagaki, S. Guan, T. Ohsuna and O. Terasaki, *Nature (London)*, 2002, **416**, 304.
36 K. N. Sandhage, M. B. Dickerson, P. M. Huseman, M. A. Caranna, J. D. Clifton, T. A. Bull, T. J. Heibel, W. R. Overton and M. E. A. Schoenwalder, *Adv. Mater.*, 2002, **14**, 429.